Journal of Solid State Chemistry **158,** 358–362 (2001)
doi:10.1006/jssc.2001.9131, available online at http://www.idealibrary.com on IDEAL®

Hydrothermal Syntheses and Crystal Structure of $NH_4Ln_3F_{10}$ (Ln = Dy, Ho, Y, Er, Tm)

Z. J. Kang,[1] Y. X. Wang, F. T. You, and J. H. Lin[2]

State Key Laboratory of Rare Earth Materials Chemistry and Applications, Department of Materials Chemistry, Peking University, Beijing 100871, People's Republic of China

Received October 23, 2000; in revised form January 26, 2001; accepted February 15, 2001

Ammonium rare earth fluorides $NH_4Ln_3F_{10}$ (Ln = Dy, Ho, Y, Er, Tm) were synthesized by a hydrothermal method. Two polymorphs, of the hexagonal β-KYb_3F_{10} and the cubic γ-KYb_3F_{10} structure types, were formed under hydrothermal conditions for most of the rare earth fluorides except $NH_4Dy_3F_{10}$, for which only the cubic γ-phase was obtained. The crystal structures of MLn_3F_{10} (M = alkaline metal, NH_4^+ and Ln = rare earth) show a strong correlation to the ratio of ionic radii (R_M/R_{Ln}), which has been expressed in a structure phase diagram of the ionic radii of univalent and rare earth cations.

Key Words: **ammonium rare earth fluorides; hydrothermal syntheses; structure phase diagram; ratio of ionic radii.**

INTRODUCTION

γ-KYb_3F_{10} crystallizes in a fluorite-related cubic structure that consists of two different structure units, $[KYb_3F_8]^{2+}$ and $[KYb_3F_{12}]^{2-}$. These two ionic groups alternate along the three crystallographic axes, forming multiple face-centered unit cells (1, 2). The coordination of the Yb^{3+} ions in the γ-KYb_3F_{10} structure is square antiprismatic. In addition to the γ-form, a high-temperature hexagonal β-form is also known for KYb_3F_{10}. In the β-KYb_3F_{10} structure, eight fluorine atoms with a bicapped trigonal prismatic geometry (3) coordinate rare earth ions. Recently, considerable interest has been focused on using these materials as hosts of solid state lasers [4–7]. Heyde *et al.* (4) studied the spectroscopic properties of the Er^{3+}-doped cubic KY_3F_{10} material and formulated the crystal field parameters. The absorption and fluorescence spectra of $KY_3F_{10}:Er^{3+}$ were reported by Antic-Fidance *et al.* (5). Electric conductivity and dielectric properties of KY_3F_{10} were also investigated (6, 7).

MLn_3F_{10} is a typical ionic family that consists of a large number of compounds; therefore, there is available considerable structural information, allowing us to rationalize the influence of the atomic parameters on the structural preference. For example, KY_3F_{10} (4–9), KTb_3F_{10} (2, 10), and $RbEu_3F_{10}$ (11) were found only in the cubic γ-form; meanwhile, the compounds with larger alkaline metals are often present in the hexagonal β-form, such as $RbLn_3F_{10}$ (Ln = Y, Er, Lu, and Sc) (11–15) and $CsLn_3F_{10}$ (Ln = Yb, Lu, and Sc) (15–19). There are indeed some examples in which both polymorphs (β- and γ-forms) were found to be stable in different temperature ranges, as found in KYb_3F_{10} (1), KEr_3F_{10} (20), and $RbGd_3F_{10}$ (11, 21–23).

Regarding the ionic radii and crystal structure of the MLn_3F_{10} family, ammonium compounds are particularly interesting, because the ionic radius (Pauling) of ammonium (1.48 Å) (24–27) is comparable with those of K^+ (1.33 Å) and Rb^+ (1.48 Å). Zalkin and Templeton (28) reported that cubic $NH_4Ho_3F_{10}$, $NH_4Er_3F_{10}$, and $NH_4Tm_3F_{10}$ could be obtained by precipitation from a solution containing ammonium ions; they described the crystal structure as the primary fluorite type. Nevertheless, the ammonium compounds cannot be obtained by conventional solid state reaction due to decomposition at high temperature. Recently Zhao *et al.* (29–31) proposed that oxygen-free complex fluorides could be prepared by hydrothermal synthesis at 140–240°C. In this paper, we present a systematic study on hydrothermal syntheses and structural characterization of $NH_4Ln_3F_{10}$.

EXPERIMENTAL

The starting materials used in hydrothermal syntheses are NH_4HF_2 (A.R.), and Ln_2O_3 (99.99%). For a typical synthetic procedure, 0.6775 g of Y_2O_3, 1.026 g of NH_4HF_2, and 30 ml of distilled water were mixed and stirred for 1 h and the pH value of the initial mixture was about 3–4. In

[1] On leave from College of Science and Technology, Yanbian University, Yanji 133002, People's Republic of China.

[2] To whom correspondence should be addressed. Fax: (8610) 62751708. E-mail: jhlin@chem.pku.edu.cn.

0022-4596/01 $35.00

some trials, a small amount of HNO_3 or ammonium hydroxide was used to adjust the pH value of the initial mixture in order to optimize the reaction conditions. The mixture was sealed in a Teflon-lined stainless-steel autoclave and heated at about 160–200°C for 4–5 days. After the mixture was washed with distilled water, polycrystalline products were recovered and dried at 110°C for 1 h. Similar hydrothermal reactions were applied to the other rare earths systems (La, Nd, Eu, Gd, Dy, Ho, Er, Tm).

X-ray powder diffraction patterns were recorded on a Rigaku D/max-2000 diffractometer using CuKα radiation source. The morphology of the samples was examined with a Hitachi S-450 scanning electron microscope. The content of hydrogen and nitrogen in the products was analyzed by using a Vario EL element analyzer. TGA analyses were carried out on a Universal V2.5H TA instrument.

RESULTS AND DISCUSSION

To optimize hydrothermal reaction conditions, the synthetic reaction of the yttrium compound $NH_4Y_3F_{10}$ was studied systematically. The synthetic reaction of $NH_4Y_3F_{10}$ under hydrothermal conditions can be expressed as

$$18NH_4HF_2 + 3Y_2O_3 \xrightarrow{H_2O} 2NH_4Y_3F_{10} + 16NH_4F + 9H_2O. \quad [1]$$

As the reaction takes place, the pH value of the system increases; therefore, the final pH values were also measured and are listed in Table 1. In most of trials, the product contains both cubic (γ-) and hexagonal (β-) forms of $NH_4Y_3F_{10}$. Figure 1a shows the X-ray powder diffraction pattern of a typical product that consists of both cubic and hexagonal $NH_4Y_3F_{10}$. Carefully adjusting the reaction conditions may yield almost pure cubic phase as shown in Fig. 1b. Elemental analysis of the cubic $NH_4Y_3F_{10}$ phase yields N, 2.96 wt% (calcd 2.949 wt%), and H, 1.23 wt% (calcd 0.80 wt%).

In addition to $NH_4Y_3F_{10}$, YF_3 was also present in some samples, which can be expressed as

$$6NH_4HF_2 + Y_2O_3 \xrightarrow{H_2O} 2YF_3 + 6NH_4F + 3H_2O. \quad [2]$$

Table 1 also lists the hydrothermal conditions and the phases in the products. The ratio of phases in the products was estimated from the relative integral intensity of the highest X-ray reflection in each phase. It can be seen that the products depend strongly on the reaction conditions, of which the initial ratios of the starting materials, pH of the reaction system, and reaction temperature are crucial. A low pH of about 1–2 leads to mainly YF_3. Cubic and hexagonal $NH_4Y_3F_{10}$ were formed in the range of pH 2–9; the hexagonal phase is, however, preferentially formed at lower temperature and higher pH. We have not yet isolated a

TABLE 1
Reaction Conditions and Products of Hydrothermal Syntheses for $NH_4Y_3F_{10}$

Starting ratio			pH,		Time	
NH_4HF_2	Y_2O_3	H_2O	s/f[a]	T (°C)	(days)	Phases in products
6	1	700	< 1/1	215	5	YF_3
6	1	560	< 1/1	195	5	YF_3
5	1	1120	1/2	195	4	YF_3
6	1	560	2/2	215	6	0.92 γ-$NH_4Y_3F_{10}$ + 0.08 β-$NH_4Y_3F_{10}$
6	1	1120	2/2	195	4	0.57 γ-$NH_4Y_3F_{10}$ + 0.06 β-$NH_4Y_3F_{10}$ + 0.37 YF_3
6	1	700	2/3	195	4	0.88 γ-$NH_4Y_3F_{10}$ + 0.06 β-$NH_4Y_3F_{10}$ + 0.06 YF_3
6	1	560	2/3	195	6	γ-$NH_4Y_3F_{10}$ + < 0.01 β-$NH_4Y_3F_{10}$
4	1	560	2/3	195	4	0.70 γ-$NH_4Y_3F_{10}$ + 0.08 β-$NH_4Y_3F_{10}$ + 0.22 YF_3
6	1	560	3/4	240	3.5	0.93 γ-$NH_4Y_3F_{10}$ + 0.07 β-$NH_4Y_3F_{10}$
6	1	560	3/4	223	5.5	γ-$NH_4Y_3F_{10}$ + < 0.01 β-$NH_4Y_3F_{10}$
6	1	560	3/4	180	3.5	γ-$NH_4Y_3F_{10}$ + < 0.01 β-$NH_4Y_3F_{10}$
6	1	330	3/4	180	15	0.85 γ-$NH_4Y_3F_{10}$ + 0.15 β-$NH_4Y_3F_{10}$
6	1	560	3/4	160	3.5	0.70 γ-$NH_4Y_3F_{10}$ + 0.30 β-$NH_4Y_3F_{10}$
6	1	560	3/4	140	3.5	0.78 γ-$NH_4Y_3F_{10}$ + 0.22 β-$NH_4Y_3F_{10}$
6	1	1120	3/4	180	15	0.93 γ-$NH_4Y_3F_{10}$ + 0.07 β-$NH_4Y_3F_{10}$
6	1	280	3/5	215	8	0.87 γ-$NH_4Y_3F_{10}$ + 0.13 β-$NH_4Y_3F_{10}$
6	1	550	3/5	180	7.5	0.94 γ-$NH_4Y_3F_{10}$ + 0.06 β-$NH_4Y_3F_{10}$
6	1	560	3/7	170	5	0.93 γ-$NH_4Y_3F_{10}$ + 0.07 β-$NH_4Y_3F_{10}$
5	1	186	3/9	215	8	0.78 γ-$NH_4Y_3F_{10}$ + 0.22 β-$NH_4Y_3F_{10}$
5	1	280	3/9	215	8	0.86 γ-$NH_4Y_3F_{10}$ + 0.14 β-$NH_4Y_3F_{10}$
4	1	560	4/9	180	3.5	0.94 γ-$NH_4Y_3F_{10}$ + 0.06 β-$NH_4Y_3F_{10}$

[a] Starting (s) and final (f) pH values.

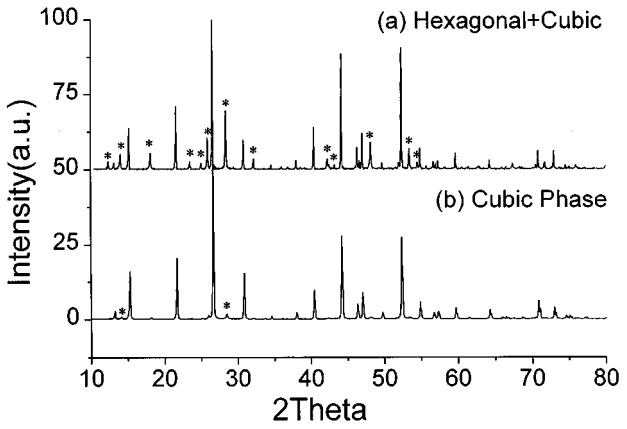

FIG. 1. X-ray diffraction patterns of $NH_4Y_3F_{10}$. (a) The product contains both cubic (γ-) and hexagonal (β-) phases; the reflections from the hexagonal $NH_4Y_3F_{10}$ are marked by $*$. (b) The product contains mainly cubic $NH_4Y_3F_{10}$.

single-phase product of the hexagonal phase, but the most abundant hexagonal $NH_4Y_3F_{10}$ (about one-third) was obtained at 160°C and pH of 3–4.

F^- ion is an effective mineralizer (30) in hydrothermal syntheses of metal fluorides. NH_4HF_2 in this case acts as both reactant and mineralizer. Therefore, excess NH_4HF_2 is required for the formation of $NH_4Y_3F_{10}$. However, under hydrothermal conditions, the solubility and its temperature coefficient may influence the crystallinity of different phases in the product more strongly. The hexagonal $NH_4Y_3F_{10}$ was often found in well-crystallized hexagonal platelike crystals (~ 10 μm) as shown in Fig. 2a. While the crystal size of the cubic $NH_4Y_3F_{10}$ is much smaller (<1 μm) as shown in Fig. 2b, the two polymorphs could be separated mechanically in some cases.

Both cubic and hexagonal $NH_4Y_3F_{10}$ decompose at high temperature. Figure 3 shows the TGA curves for the cubic phase and a product that contains about one-third of the hexagonal phase. The solid residue after decomposition is YF_3. The weight loss is almost identical for both samples, i.e., 7.75 wt% and 7.88 wt% for the cubic sample and the mixture sample, respectively, which agree very well with that expected for the decomposition of $NH_4Y_3F_{10}$ to YF_3 (7.794 wt%). The decomposition temperature is slightly different. The cubic form decomposes at about 447°C; meanwhile, the decomposition temperature increases to about 463°C for the sample that contains one-third hexagonal phase. X-ray powder diffraction shows that the phase ratio of $R_{ph} = \beta\text{-}NH_4Y_3F_{10}/\gamma\text{-}NH_4Y_3F_{10}$ (β/γ) increases after annealing of the mixture sample at 400°C for 1.5 h, which might be an indication that the hexagonal $NH_4Y_3F_{10}$ is a more stable form at higher temperature.

Rietveld refinement on a cubic sample confirmed that the cubic $NH_4Y_3F_{10}$ crystallizes in the γ-KYb_3F_{10} structure type ($R_p = 0.076$, $R_{wp} = 0.11$ and $R_B = 0.038$). A small amount of the hexagonal phase was present in this sample, which was also refined by Rietveld refinement. The lattice constants of $NH_4Y_3F_{10}$ are $a = 11.5846(1)$ Å for the cubic form and $a = 8.195(1)$ Å, $c = 13.396(6)$ Å for the hexagonal form. Table 2 listed the refined structure parameters.

The above results demonstrate that the hydrothermal technique is a promising method for synthesis of the am-

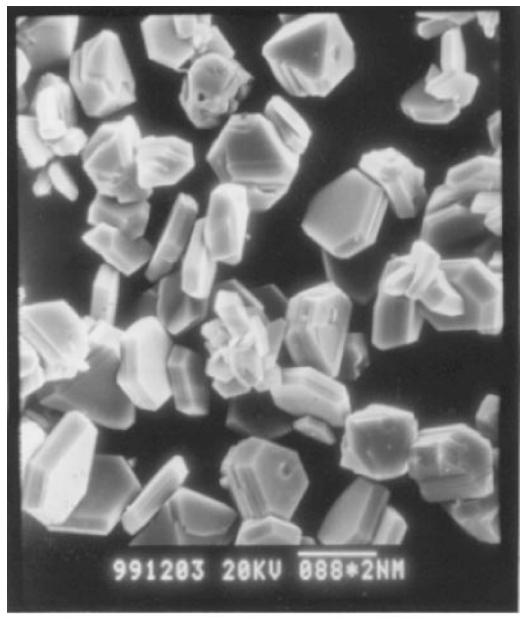

(a) Hexagonal $NH_4Y_3F_{10}$

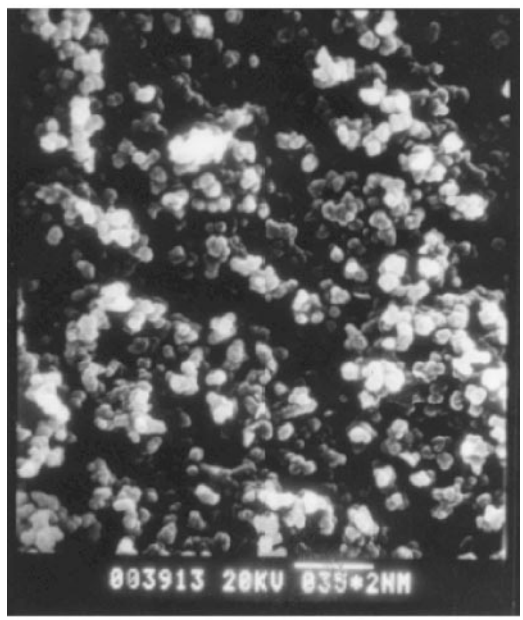

(b) Cubic $NH_4Y_3F_{10}$

FIG. 2. Electron scanning microscopic view of (a) hexagonal and (b) cubic $NH_4Y_3F_{10}$.

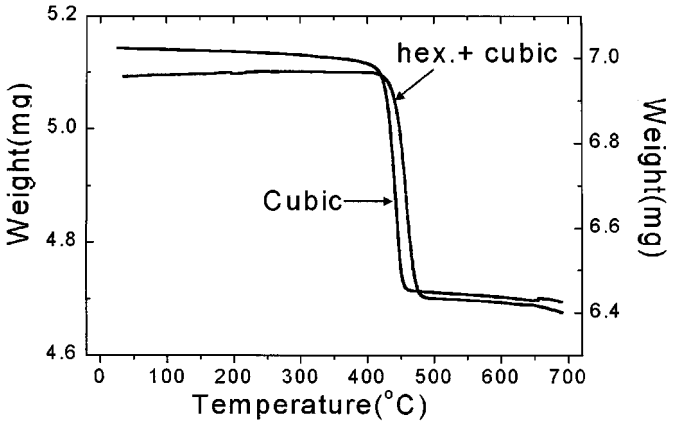

FIG. 3. TGA curves of a pure cubic γ-$NH_4Y_3F_{10}$ phase and a product that contains about one-third hexagonal phase and two-thirds cubic phase, during which the reaction $NH_4Y_3F_{10} \xrightarrow{\Delta} 3YF_3 + NH_3\uparrow + HF\uparrow$ took place.

TABLE 3
Reaction Conditions[a] and Products of Hydrothermal Syntheses for $NH_4Ln_3F_{10}$ (Ln = La, Nd, Eu, Gd, Dy, Ho, Er, Tm)

	Starting ratio			
System	NH_4HF_2	Ln_2O_3	H_2O	Phases in product
La	6	1	560	LaF_3
Nd	6	1	560	NdF_3
Eu	6	1	560	EuF_3
Gd	6	1	560	GdF_3
Dy	6	1	560	γ-$NH_4Dy_3F_{10}$
Ho	6	1	560	β-$NH_4Ho_3F_{10}$/ γ-$NH_4Ho_3F_{10}$ = 0.20
Er	6	1	560	β-$NH_4Er_3F_{10}$/ γ-$NH_4Er_3F_{10}$ = 1.0
Tm	6	1	560	β-$NH_4Tm_3F_{10}$/ γ-$NH_4Tm_3F_{10}$ = 1.5

[a] The pH of the system was 3–4 and the reaction was carried out at 200°C for 4 days.

monium rare earth fluorides $NH_4Ln_3F_{10}$. To see the influence of ionic size on the crystal structure, similar hydrothermal reactions were applied to the other rare earth systems (La, Nd, Eu, Gd, Dy, Ho, Er, Tm). Table 3 lists the reaction conditions and products obtained in these systems. It was found that the light rare earth elements tend to form LnF_3 (Ln = La, Nd, Eu, Gd), instead of $NH_4Ln_3F_{10}$. This does not mean that the light rare earth elements cannot form $NH_4Ln_3F_{10}$ compounds; they are, at least, less stable under the present synthetic conditions. Meanwhile, $NH_4Ln_3F_{10}$ was obtained for the heavy rare earth systems (Ln = Dy, Ho, Er and Tm); more interestingly, the phase ratio ($R_{ph} = \beta/\gamma$) exhibits a variation trend, from almost pure γ-form for $NH_4Dy_3F_{10}$ to majority β-form for $NH_4Tm_3F_{10}$.

Figure 4 shows a structure phase diagram for MLn_3F_{10} as a function of the ionic radii of univalent and rare earth ions (1–23, 32–35). In this figure, we summarize most of the known compounds in the MLn_3F_{10} family. $RbIn_3F_{10}$ (35), though not a rare earth compound, is included in the figure because it crystallizes also in the hexagonal β-KYb_3F_{10} structure. The hexagonal and cubic forms of MLn_3F_{10} are distinctively distributed in the structural phase diagram, indicating that the ionic radii are suitable structural parameters. The hexagonal compounds in the MLn_3F_{10} family are located mostly in the upper-left region of the phase diagram and the cubic compounds are mostly in the lower-right region. This means that the hexagonal structure prefers to have a larger R_M/R_{Ln} ratio and the cubic structure is predominant for smaller R_M/R_{Ln} ratio systems. The straight line in the figure separates roughly the two structure types in the phase diagram, with compounds close to the boundary often present in both polymorphs.

The R_M/R_{Ln} ratios of ammonium and heavy rare earth ions are all close to the phase boundary; therefore, both of the hexagonal and cubic forms coexist in the products. In

TABLE 2
Structure Parameters of γ-$NH_4Y_3F_{10}$

Atom	x	y	z	B
Y1	0	0.2400 (1)	0	0.11 (2)
N1	$\frac{1}{4}$	$\frac{1}{4}$	$\frac{1}{4}$	0.12 (17)
F1	0.1121 (2)	x	x	0.13 (5)
F2	$\frac{1}{2}$	0.3332 (2)	y	0.13 (5)

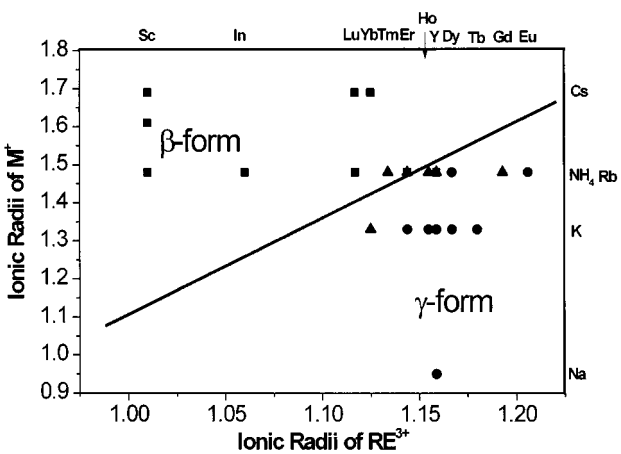

FIG. 4. Structure phase diagram for MLn_3F_{10} as a function of the ionic radii of univalent and rare earth ions. The solid line in the figure roughly separates γ- and β-form phase regions; the symbol ■ represents the compounds that crystallize only in the hexagonal β-structure, ● in the cubic γ-structure, and ▲ in both hexagonal β- and cubic γ-structures.

addition, the phase ratio ($R_{ph} = \beta/\gamma$) of the different systems is indicative of the stability of different structure types. For example, almost pure γ-form was obtained for the largest heavy rare earth system studied (Dy^{3+}). As the ionic radius of rare earths decreases, the phase ratio ($R_{ph} = \beta/\gamma$) increases, and thereafter the β-form becomes predominant in the $NH_4Tm_3F_{10}$ system. Finally, the phase diagram could be used to predict the possible structure type of the unknown MLn_3F_{10} compounds. For example, the compounds of rubidium with light rare earth ions, such as $RbLn_3F_{10}$ (Ln = La, Nd, etc.), should crystallize in the cubic γ-structure, while $RbYb_3F_{10}$ and $RbLu_3F_{10}$ may be present in both β- and γ-polymorphs.

In conclusion, we show that the hydrothermal technique is a promising method for synthesis of ammonium rare earth fluorides $NH_4Ln_3F_{10}$ (Ln = Dy, Ho, Er, Tm, and Y). Most of the ammonium compounds of $NH_4Ln_3F_{10}$ crystallize in both β- and γ-polymorphs, because the ionic radii ratios R_M/R_{Ln} of ammonium and heavy rare earth ions are close to the phase boundary between the hexagonal and cubic forms. In addition, the structure preference of the compounds in the MLn_3F_{10} family can be interpreted empirically on the basis of the ionic radii of alkaline metals and rare earths.

ACKNOWLEDGMENTS

We are thankful for financial support from NSFC (29971002), Rhodia Rare Earth Co., and the State Key Basic Research Program (G1998061306).

REFERENCES

1. M. Labeau, S. Aleonard, A. Vedring, R. Boutonnet, and J. C. Cousseins, *Mater. Res. Bull.* **9,** 615–624 (1974).
2. D. J. M. Bevan, O. Greis, and J. Staehle, *Acta Crystallogr. A* **36,** 889–890 (1980).
3. P. S. Aleonard, J. C. Guitel, Y. L. Fur, and M. T. Roux, *Acta Crystallogr. B* **32,** 3227–3235 (1976).
4. K. Heyde, K. Binnemans, and C. Gorller-Walrand, *J. Chem. Soc., Faraday Trans.* **94,** 1671–1674 (1998).
5. E. Antic-Fidance, M. Lemaitre-Blaise, and P. Porcher, *in* "Rare Earths Spectroscopy" (B. Jezowska-Trebiatowska, J. Legendziewicz, and W. Strek, Eds.), pp. 134–145. World Scientific, Singapore, 1985.
6. A. P. Ayala, M. A. S. Oliveira, J. Y. Gesland, and R. L. Moreira, *J. Phys.: Condens. Matter* **10,** 5161–5170 (1998).
7. N. F. Yvarov and E. F. Hairetdinov, *Solid State Ionics* **36,** 29 (1989).
8. D. J. M. Bevan and S. E. Lawton, *Acta Crystallogr. B* **42,** 55–58 (1986).
9. J. W. Pierce and H. Y. P. Hong, *in* "Proceeedings of the Tenth Rare-earth Research Conference" (C. J. Kevan, Ed.), pp. 527–537. U.S. Atomic Energy Commission, Technical Information Center, Washington, DC, 1973.
10. N. V. Podberezskaya, O. G. Potapova, S. V. Borisov, and Yu. V. Gatilov, *J. Struct. Chem.* **17,** 948–950 (1976).
11. M. Tachihante, M. T. Founier, A. Arbus, and J. C. Cousseins, *Solid State Commun.* **51,** 577–580 (1984).
12. J. Chassaing, *J. Inorg. Nucl. Chem.* **37,** 1554–1556 (1975).
13. S. Aleonard, O. Gonzales, M. F. Gorius, and M. T. Roux, *Mater. Res. Bull.* **10,** 1185–1192 (1975).
14. A. Arbus, M. T. Fournier, J. C. Cousseins, A. Vedrine, and R. Chevalier, *Acta Crystallogr. B* **38,** 75–79 (1982).
15. J.-C. Champarnaud-Mesjard and B. Frit, *J. Less-Common Metals* **167,** 319–327 (1991).
16. S. Aleonard, M. T. Roux, and B. Lambert, *J. Solid State Chem.* **42,** 80–88 (1982).
17. S. Aleonard, M. F. Gorius, and M. T. Roux, *Mater. Res. Bull.* **17,** 1251–1263 (1982).
18. J. Metin, D. Avignant, and J. C. Cousseins, *Rev. Chim. Miner.* **24,** 267 (1987).
19. R. E. Marsh, *J. Solid State Chem.* **47,** 242–243 (1983).
20. S. Aleonard, J. C. Guitel, and M. T. Roux, *J. Solid State Chem.* **24,** 331–344 (1978).
21. A. Arbus, M. T. Fournier, and A. Vedrine, *Mater. Res. Bull.* **18,** 135–140 (1983).
22. R. Mahiou, J. Metin, D. Zambon, A. Arbus, M. T. Fournier, and J. C. Cousseins, *Inorg. Chim. Acta* **139,** 265–267 (1987).
23. J. Metin, R. Mahiou, M. T. Fournier, and J. C. Cousseins, *Mater. Res. Bull.* **22,** 1131–1136 (1987).
24. An inconsistency was found for the ionic radius of NH_4^+ in the literature. The reported NH_4^+ radius ranges from 1.48 Å (Pauling radius) to 1.75 Å (25–27). This inconsistency may originate from the presence of hydrogen bonding and the polyatomic nature of the NH_4^+ ion. Nevertheless, it was commonly accepted that the ionic radius of NH_4^+ is comparable with those of K^+ and Rb^+. Therefore, the Pauling ionic radii of $Na^+ = 0.95$ Å, $K^+ = 1.33$ Å, $NH_4^+ = 1.48$ Å, $Rb^+ = 1.48$ Å, and $Cs^+ = 1.61$ Å (25) were used in this study, although we believe that the ionic radius of NH_4^+ should be smaller in fluorides because of a stronger hydrogen bond. The crystal ionic radii of the rare earth cations were obtained from Ref. (26).
25. F. A. Cotton, G. Wilkinson, C. A. Murillo, and M. Bochmann, "Advanced Inorganic Chemistry," 6th Ed., pp. 1302–1304. Wiley, New York, 1999.
26. R. B. King, "Encyclopedia of Inorganic Chemistry," Vol. 2, pp. 929–941. Wiley, New York, 1994.
27. J. E. Huheey, "Inorganic Chemistry," 3rd Ed., pp. 76–78. Harper International SI Edition, New York, 1983.
28. A. Zalkin and D. H. Templeton, *J. Am. Chem. Soc.* **75,** 2453–2458 (1953).
29. X. M. Xun, S. H. Feng, J. Z. Wang, and R. R. Xu, *Chem. Mater.* **9,** 2966–2968 (1997).
30. Z. Shi and S. H. Feng, *Chem. J. Chinese Univ.* **20,** 172–175 (1999).
31. C. Y. Zhao, S. H. Feng, R. R. Xu, C. S. Shi, and J. Z. Ni, *Chem. Commun.* 945–946 (1997).
32. P. Valon, J. C. Gacon, A. Vedrine, and G. Boulon, *J. Solid State Chem.* **21,** 357–369 (1977).
33. A. Arbus, M. T. Fournier, B. Picaud, G. Boulon, and A. Vedrine, *J. Solid State Chem.* **31,** 11–21 (1980).
34. G. Grenet and M. R. Kibler, *J. Solid State Chem.* **23,** 1–10 (1978).
35. J. C. Champarnaud-Mesjard, D. Mercurio, and B. Frit, *J. Inorg. Nucl. Chem.* **39,** 947–951 (1977).